HEFAT2010
7th International Conference on Heat Transfer, Fluid Mechanics and Thermodynamics
19-21 July 2010
Antalya, Turkey

NUMERICAL ANALYSIS OF TRANSIENT HEAT TRANSFER BY THERMOCAPILLARY FLOW AROUND A NON-CONDENSABLE GAS BUBBLE ON A HEATED WALL

Lamas, M.I.*, Sáiz Jabardo, J.M., Arce, A.
*Author for correspondence
Departamento de Construcciónes Navais,
Escola Politécnica Superior,
Universidade da Coruña,
Mendizábal s/n 15403, Ferrol, A Coruña,
Spain,
E-mail: isabellamas@udc.es

ABSTRACT

It has been argued in the past that thermocapillary induced liquid motion related to the bubbles on the heated wall, also known as Marangoni flow, could be a significant heat transfer mechanism in nucleate boiling. Thermocapillary flows have been under intense scrutiny in the past. However, their influence in nucleate boiling heat transfer is still sketchy. The present paper reports the results of an investigation of the effect on the heat transfer rate of thermocapillarity induced flow by the presence of a hemispherical non-condensable gas bubble on a heated wall. Transient solutions of the governing field equations in a domain containing the hemispherical non-condensable gas bubble have been obtained through a commercial CFD program. The considered domain included the heated wall, the bubble and the liquid, assumed to have infinite extent. The non-dimensional governing groups are the Rayleigh, the Prandtl, and the Marangoni numbers, which, in the present investigation, varied in the following ranges: $0 \leq Ra \leq 5X10^3$, $4.5 \leq Pr \leq 220$, and $10^3 \leq Ma \leq 10^5$. Temperature and flow fields have been obtained for three bubble orientations: upward, downward, and lateral. As should be expected, the temperature and the flow fields are governed by thermocapillary and buoyancy effects. Since the liquid is initially at a uniform temperature, the presence of the bubble and the heated wall, either at a different temperature or at an imposed heat flux, causes a burst of thermocapillary flow in the form of a jet of warm liquid streaming out of the wall. Present results compare reasonably well with experimental ones obtained elsewhere for downward and laterally facing bubbles.

INTRODUCTION

Nucleate boiling has been investigated since the thirties of the last century and is characterized by high heat transfer coefficients. One of the main concerns regarding the investigation of nucleate boiling heat transfer has been the determination of the intervening heat transfer mechanisms. Several heat transfer mechanisms have been proposed such as local convection, micro-convection, micro-layer evaporation, transient conduction, and thermocapillarity. The thermocapillarity phenomenon was discovered by the Italian scientist Carlo Marangoni in mid 19th Century, hence it is also known as Marangoni effect. The term thermocapillarity is used in regards to the fluid movement caused by surface tension gradients related to corresponding temperature gradients along a liquid-gas interface. Since higher surface tension regions of an interface tend to contract more than the lower surface tension ones, shear stresses are promoted in the competing phases, dragging both gas and liquid toward the regions of higher surface tension or lower temperature.

Thermocapillarity has been increasingly investigated since Brown [1] published his doctoral thesis in 1967. Brown suggested that thermocapillarity could be one of the heat transfer mechanisms in nucleate boiling. Formerly, several researchers had investigated thermocapillary flows. Young [2] carried out an investigation of the movement of a bubble in a non-uniform temperature medium. Trefethen [3] obtained movie pictures of jets streaming out of bubbles on a heated wire. Farello [1] obtained excellent pictures of liquid jets around bubbles on a heated wire. **Figure 1 (a)** illustrates a colored Schlieren picture of jets around bubbles on heated wire immersed in distilled water [1]. Other interesting photographic research was done by McGrew [4]. The picture of **Figure 1 (b),** taken by the second author, shows liquid jets streaming out of bubbles on a quasi vertical platinum wire.

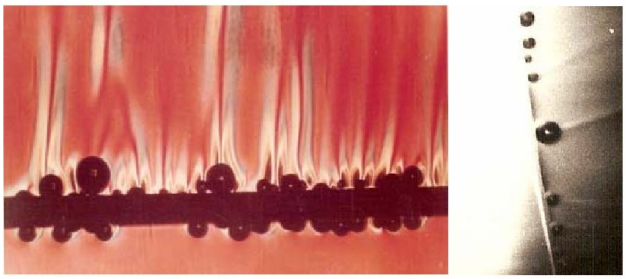

(a) (b)

Figure 1. Thermocapillarity phenomena taking place in hot wires: (a) horizontal, colored Schlieren [1]; (b) quasi vertical, shadow effect.

The first numerical studies of the thermocapillariy phenomenon appeared during the seventies of the last century. The first relevant numerical work was due to Larkin [5], who investigated the phenomenon around a bubble attached to a heated wall. Later, Gaddis [6] developed a numerical analysis of Marangoni flow around a vapor bubble. He concluded that, under partial nucleate boiling conditions, when the heated surface is covered by a sparse bubble population, thermocapillarity could be an important heat transfer mechanism. Kao and Kenning [7] worked with vapor bubbles and non-condensable gas bubbles and confirmed Gaddis results. Sáiz Jabardo and Jones [8] also developed a transient numerical model to study thermocapillarity around a non-condensable gas bubble.

Straub *et al.* [9-12] published several numerical studies of thermocapillarity around bubbles. They analyzed the problem under steady and transient conditions, for both normal and micro-gravity and different geometries. They also evaluated the error by considering a two-dimensional model instead of a tri-dimensional one.

Arlabosse *et al.* [13-15] carried out a numerical-experimental research using several silicon oils of different viscosities. For the cases studied, they concluded that thermocapillarity is important in the close vicinity of the bubble but, beyond two bubble diameters, heat transfer is dominated by conduction.

Peng *et al.* [16-19] analyzed transient nucleate boiling using wires instead of cylindrical or flat heated walls. O'Shaugnessy and Robinson [20] and Radulescu and Robinson [21] reported numerical solutions for steady state involving different geometries of the bubble under normal and microgravity conditions. Recently, Lamas *et al.* [22-23] have performed a numerical investigation of thermocapillarity around hemispherical non-condensable bubbles under steady and transient conditions. Working with non-dimensional field equations, they were able to analyze the effect of the characteristic non-dimensional parameters on thermocapillary flow and heat transfer.

NOMENCLATURE

E	[m]	Width
H	[m]	Depth
g	[m/s^2]	Gravity acceleration
k	[W/mK]	Thermal conductivity
n	[ ]	Unit normal vector
s	[ ]	Unit tangential vector
p	[Pa]	Pressure
R	[m]	Bubble radius
T	[K]	Temperature
t	[s]	Time
V	[m/s]	Velocity
ΔT	[K]	T-T_{ref}
T_{ref}	[K]	Reference temperature for Boussinesq approximation

Greek symbols

α	[m^2/s]	Thermal diffusivity
β	[K^{-1}]	Thermal expansion coefficient
θ	[°]	Contact angle
σ	[N/mK]	Temperature coefficient of surface tension
Φ	[W/m^2]	Heat flux
ψ	[kg/s]	Stream function
γ	[°]	Angle around interface

Subscripts

max	Maximum
ref	Reference

Superscripts

*	Non-dimensional

Dimensionless parameters

Ma	Marangoni number, $Ma = \dfrac{\lvert\partial\sigma / \partial T\rvert \phi R^2}{k\mu\alpha}$
Pr	Prandtl number, $\mathrm{Pr} = \nu / \alpha$
Ra	Rayleigh number, $Ra = \dfrac{\beta g R^4 \phi}{k\alpha\nu}$
Nu	Nusselt number, $Nu = \dfrac{hR}{k}$

MATHEMATICAL MODEL

Problem description

The proposed model deals with a non-condensable gas bubble attached to a heated wall and immersed in an infinite liquid medium. A sketch corresponding to a downward facing bubble is shown in **Figure 2 (a)**, whereas **Figure 2 (b)** shows the detail of the bubble and the corresponding contact angle θ. The contact angle was taken as 71° for all the cases studied in this paper.

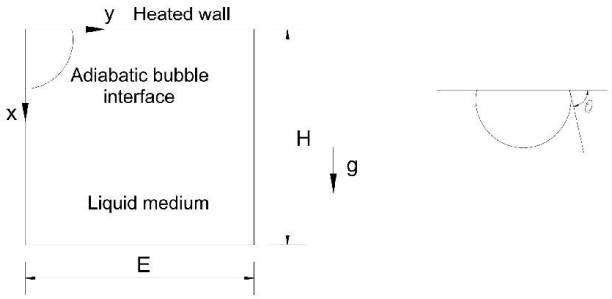

Figure 2. (a) Geometry; (b) contact angle.

The model is based on the following set of assumptions:

- Axisymmetry for downward and upward bubbles. Lateral bubbles require a tri-dimensional domain.
- Adiabatic bubble interface (non-condensable gas bubble).
- Constant bubble volume and size.
- Boussinesq approximation.
- Infinite liquid medium.
- Constant properties.
- Laminar flow.

Governing equations

The governing field equations are the conservation of mass, momentum and energy:

$$\nabla \cdot \vec{V} = 0 \tag{1}$$

$$\frac{\partial \vec{V}}{\partial t} + \nabla \cdot (\vec{V}\vec{V}) = -\frac{\nabla p}{\rho} + \nu \nabla^2 \vec{V} - \vec{g}\,\beta(T - T_{ref}) \tag{2}$$

$$\frac{\partial T}{\partial t} + \vec{V} \cdot \nabla T = \alpha \nabla^2 T \tag{3}$$

The momentum and energy boundary conditions are shown in **Table 1**.

Table 1. Boundary conditions for energy and momentum equations.

Zone	Boundary condition energy eq.	Boundary condition momentum eq.
Top wall	$-k\frac{\partial T}{\partial x} = \phi$	$\vec{V} = 0$
Bottom wall	$T = 0$	$\vec{V} = 0$
Lateral wall	$\frac{\partial T}{\partial y} = 0$	$\vec{V} = 0$
Interface	$\frac{\partial T}{\partial n} = 0$	$\tau = \mu\frac{\partial \vec{V}}{\partial n} = \left\lvert\frac{\partial \sigma}{\partial T}\right\rvert\frac{\partial T}{\partial s}$
Symmetry axis†	$\frac{\partial T}{\partial n} = 0$	$\frac{\partial \vec{V}}{\partial n} = 0$

†Only for upward and downward bubbles.

Dimensionless field equations have been obtained by introducing the reference parameters shown in **Table 2**. The dimensionless variables, quoted with a "*", are also shown in this table.

The resulting field equations in dimensionless form are as follows:

$$\nabla \cdot \vec{V}^* = 0 \tag{4}$$

$$\frac{\partial \vec{V}^*}{\partial t^*} + \nabla \cdot (\vec{V}^*\vec{V}^*) = -\nabla p^* + \mathrm{Pr}\,\nabla^2 \vec{V}^* - Ra\,\mathrm{Pr}\,T^*\frac{\vec{g}}{g} \tag{5}$$

$$\frac{\partial T^*}{\partial t^*} + \vec{V}^* \cdot \nabla T^* = \nabla^2 T^* \tag{6}$$

Table 2. Reference parameters.

Dimension	Reference parameter	Dimensionless parameter
Length	$L_{ref} = R$	$x^* = x/L_{ref}\,;\; y^* = y/L_{ref}$
Velocity	$V_{ref} = \alpha/R$	$\vec{V}^* = \vec{V}/V_{ref}$
Temperature	$\Delta T_{ref} = \phi R/k$	$T^* = \Delta T/\Delta T_{ref}$
Pressure	$P_{ref} = \rho V_{ref}^2$	$P^* = P/P_{ref}$
Time	$t_{ref} = L_{ref}/V_{ref} = R^2/\alpha$	$t^* = t/t_{ref}$

The non-dimensional groups associated to the present model are the ones that appear in the dimensionless momentum equation, namely the Rayleigh number, which corresponds to the ratio between buoyancy and heat diffusion effects, and the Prandtl number, which is a transport property of the liquid. An additional dimensionless characteristic group results in connection with the non-dimensional form of the momentum interface boundary condition, shown in **Table 3,** which includes the dimensionless boundary conditions corresponding to **Table 1**. The additional dimensionless group is the Marangoni number, which represents the ratio between surface tension and viscous effects at the liquid-gas interface.

Table 3. Boundary conditions for energy and momentum equations in dimensionless form.

Zone	Boundary condition energy eq.	Boundary condition momentum eq.
Top wall	$\frac{\partial T^*}{\partial x^*} = -1$	$\vec{V}^* = 0$
Bottom wall	$T^* = 0$	$\vec{V}^* = 0$
Lateral wall	$\frac{\partial T^*}{\partial y^*} = 0$	$\vec{V}^* = 0$
Interface	$\frac{\partial T^*}{\partial n^*} = 0$	$\frac{\partial \vec{V}^*}{\partial n^*} = Ma\frac{\partial T^*}{\partial s^*}$
Symmetry axis†	$\frac{\partial T^*}{\partial n^*} = 0$	$\frac{\partial \vec{V}^*}{\partial n^*} = 0$

†Only for upward and downward bubbles.

NUMERICAL PROCEDURE

The governing equations were solved using the commercial software Ansys Fluent 6.3 [24], which is based on the control volume method. The domain was discretized by tetrahedral elements, using a thinner size mesh near the heat source (0.1 non-dimensional units) and coarser beyond the heat source (0.5 non-dimensional units).

The velocity-pressure coupling in the discretized momentum equations was handled using the SIMPLE (Semi-Implicit Method for Pressure-Linked Equations) algorithm. An implicit method was used to avoid numerical oscillations which deteriorate convergence.

For downward and upward bubbles, the problem was solved as a two-dimensional axisymmetric domain. For the lateral bubble problem, the domain was a three-dimensional one. Though the domains were intended to represent an infinite medium, the numerical approach requires a previous procedure to determine which distance could be numerically infinite. Details of the procedure are presented elsewhere [23].

Steady state experimental results obtained by Arlabosse *et al.* [15] have been used to validate the proposed model and its numerical solution. Details of the validation procedure can be found in [22].

RESULTS AND DISCUSSION

Velocity field

The stream lines of the flow field will be considered first. **Figure 3** plots display streamlines for different bubble configurations and different Marangoni and Rayleigh numbers at a dimensionless time of 0.2 and Prandtl number of 4.5. In the case of a downward facing bubble, after an initial burst of thermocapillary flow as a strong downward jet of warm liquid, generating a counter clockwise vortex, buoyancy effects act over the expelled warm liquid forcing the formation of a second clockwise vortex. As a result, at later times, as in **Figure 3 (a)**, two or more vortices set in. A weak counter clockwise thermocapillary propelled vortex sets in close to the bubble interface whereas further away a stronger clockwise buoyancy induced vortex can be noted in that figure. Though not present at the time of the plot of **Figure 3 (a)**, several buoyancy driven, weak vortices, form at later times.

Figure 3 (b) displays the flow field for a bubble in microgravity ($g \approx 0$). In this case the bubble orientation is indifferent and, as expected, thermocapillarity is the only driving force of the flow field. A strong counter clockwise vortex sets in whose center moves further away from the bubble with time. The flow field for the upward facing bubble, **Figure 3 (c)**, is similar to that under microgravity. In this case buoyancy and thermocapillarity effects enhance each other to generate a strong clockwise vortex which forces warm liquid from the wall region to regions far away from the bubble.

Contrary to the former ones, the case of a lateral bubble, **Figure 3 (d)**, does not present a spatial symmetry. As a result, as previously observed, the numerical domain is three dimensional. The resultant flow field is illustrated by the stream lines plot of **Figure 3 (d)** for the common dimensionless time of 0.2. A strong clockwise vortex, buoyancy dominated, with its center located above the bubble, sets in and interacts with a thermocapillarity driven weak one, close to the base of the bubble. Thermocapillarity effects induce the strong vortex formation due to their characteristic tendency to move the liquid away from the wall.

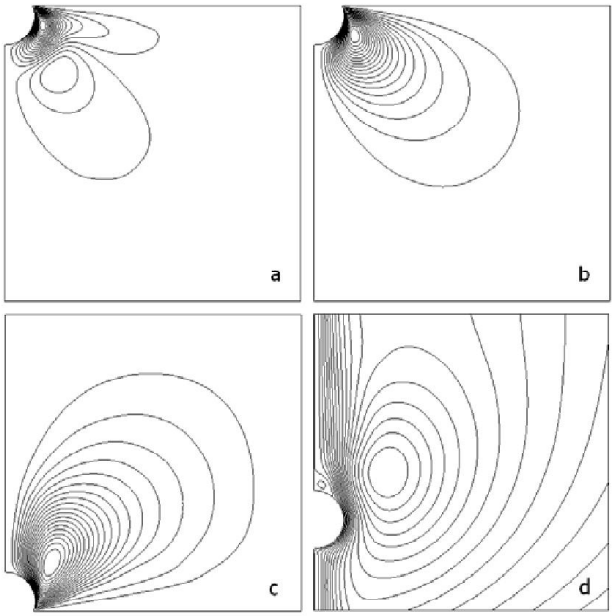

Figure 3. Stream lines for t*=0.2 and Pr=4.5. (a) Ma=10,000, Ra=5,000, downward bubble; (b) Ma=10,000, Ra=0; (c) Ma=10,000, Ra=5,000, upward bubble; (d) Ma=10,000, Ra=5,000, lateral bubble.

The "jet strength" is defined as the maximum value of the stream function in the vortex, ψ_{max}. Its value could be considered as way of quantifying the vortex strength. The variation of the jet strength (strong vortex) with time for the case of the lateral bubble is shown in **Figure 4** for different values of the Marangoni number and the same Prandtl and Rayleigh numbers of **Figure 3 (d)**. As expected, the jet strength increases with the Marangoni number and time, as clearly shown in **Figure 4**. It has been shown in a previous study [23] that the jet strength is weakly affected by the Prandtl number. In addition, the center of the thermocapillarity induced vortex, where ψ_{max} is evaluated, can move with time either away or closer to the bubble, depending on the bubble orientation.

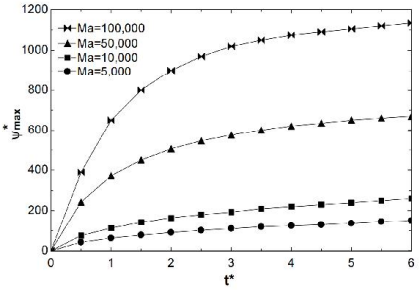

Figure 4. Jet strength for Pr = 4.5; Ra = 5,000; lateral bubble.

The maximum velocity occurs close to the bubble interface, the origin of the thermocapillarity driven flows. The interface velocity distribution for the cases of downward and upward facing bubbles has been presented in a previous paper [24]. The case of the lateral bubble is the most interesting one due to the non-symmetry that characterizes this orientation. The velocity around the interface for the lateral bubble for different times is shown in **Figure 5 (a)**, for the same conditions as in **Figure 3 (d)**. The following are general conclusions that can be drawn from this plot:

(1) The velocity at the interface increases with time since buoyancy effects tend to increase as the temperature gradients in the liquid increase from the initial zero value.

(2) The velocity increases with the position along the interface in the downward facing interface up to a maximum.

(3) The position where the maximum occurs moves to the right (higher values of γ) with time, a result which is related with the increment of the buoyancy effects with time that in this face enhance thermocapillarity effects.

(4) In the upward facing region the velocity is rather small as compared to the downward facing one as a result of opposed to each other of thermocapillarity and buoyancy effects. This effect is clearly visible in **Figure 5 (b)**, where the velocity vector distribution in the region close to the bubble is shown.

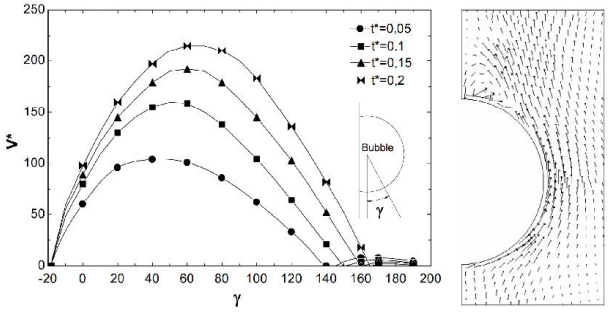

Figure 5. (a) Velocity field around interface for Ma = 10,000 ; Pr = 4.5; Ra = 5,000; lateral bubble. (b) Velocity field for Ma = 10,000; Pr = 4.5; Ra = 5,000; t*= 0.2; lateral bubble.

Temperature field

Figure 6 shows the temperature field corresponding to conditions of **Figure 3**. The following are some conclusions related to the plots of **Figure 6**.

(1) Isothermal lines tend to align perpendicularly to symmetry planes, which function as adiabatic walls, and to the bubble interface which is assumed as adiabatic.

(2) The isothermal lines tend to become parallel to the heated wall as the distance from the bubble increases as a result of a progressive fading of thermocapillarity effects.

(3) Thermocapillarity effects are clearly noticed in connection with the increment of temperature gradients related to the "packing" of isotherms in the region of the wall close to the bubble.

(4) Temperature gradients along the wall for the laterally oriented bubble are clearly larger than those for the other orientations due to buoyancy effects along the wall.

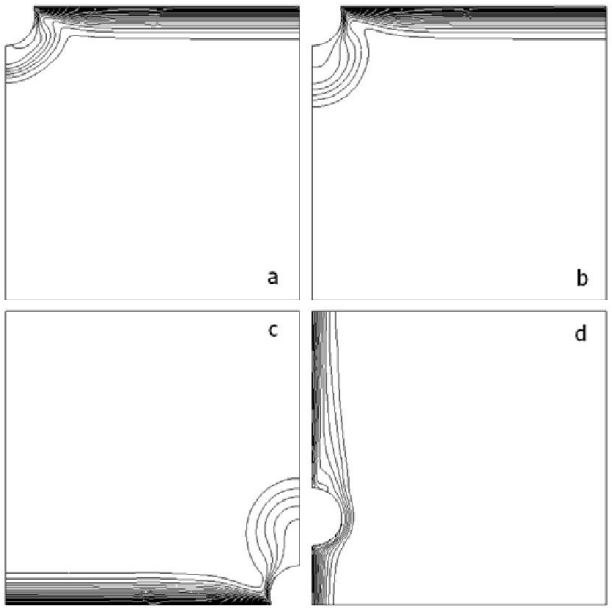

Figure 6. Temperature contours for t* = 0.2 and Pr = 4.5. (a) Ma = 10,000, Ra = 5,000, downward bubble; (b) Ma = 10,000, Ra = 0; (c) Ma = 10,000, Ra = 5,000, upward bubble; (d) Ma = 10,000, Ra = 5,000, lateral bubble.

The significance of thermocapillarity effects on the rate of heat transfer along the wall has been evaluated through the local Nusselt number. The variation of the local Nusselt number along the wall for the case of a downward facing bubble for different Marangoni numbers is presented in **Figure 7 (a)**. The isotherms corresponding to this plot are shown **in Figure 7 (b).** It can be noted that in the region close to the bubble, the Nusselt number reaches values up to 60% higher than those at the region where heat is transferred by conduction, where, as should be expected, the Nusselt number is unity.

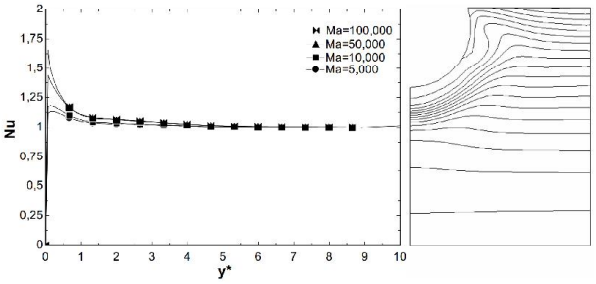

(a) (b)

Figure 7. (a) Nusselt number at the heated wall for Pr = 4.5; Ra = 5,000; t* = 0.2; downward bubble. (b) Temperature field at the heated wall for Ma = 10,000; Pr = 4.5; Ra = 5,000; t* = 0.2.

For a laterally oriented bubble, thermocapillarity effects are less important. In fact, isothermal lines are less distorted in the bubble region for a lateral bubble than for a downward bubble as can be concluded by comparing **Figure 8 (b)** with **Figure 7 (b)**. As a result, the increment in heat transfer related to

thermocapillarity effects in the case of a laterally oriented bubble is less significant than in the previous case. This trend is apparent in **Figure 8 (a)**, where a small Nusselt number increment is observed in a region of the wall very close to the bubble. In this case, buoyancy effects are clearly dominant in the heat transfer mechanism. Similar results have been obtained for the whole range of the Marangoni number considered in the present investigation, which varied from 5,000 to 100,000.

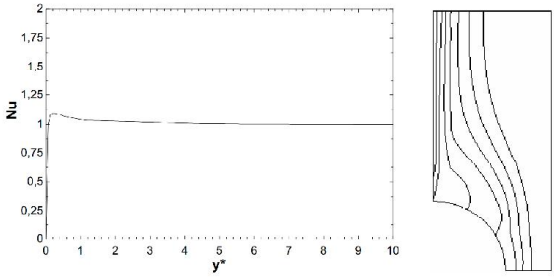

Figure 8. (a) Nusselt number at the heated wall above the bubble for Pr = 4.5; Ra = 5,000; t* = 0.2; lateral bubble. (b) Temperature at the hot wall for Ma = 10,000; Pr = 4.5; Ra = 5,000; t* = 0.2.

CONCLUSIONS

Temperature and flow fields have been obtained for three bubble orientations: upward, downward, and lateral. As should be expected, the temperature and the flow fields are governed by thermocapillary and buoyancy effects. Given that the liquid is initially at a uniform temperature, the presence of the heated wall and the bubble causes an initial burst of thermocapillary flows in the form of a jet of warm liquid normal to the heated wall. For a downward facing bubble, the warm liquid is submitted to buoyancy effects, and, as a result, the extent of the jets tends to shrink, finally affecting only the region closed to the bubble. Buoyancy and capillary effects combine to produce a strong upwards jet of warm liquid in the case of the upwards oriented bubble. Horizontal warm liquid jet progressively deviating upwards is observed when the bubble is laterally located. Convective effects promoted by thermocapillarity are limited to a region very close to the bubble, being insignificant in the case of a laterally oriented bubble, where buoyancy effects are clearly dominant.

REFERENCES

[1] Brown, W.T., 1967, A study of flow surface boiling, *Ph. D. Thesis, Massachusetts Institute of Technology, EEUU.*

[2] Young, N.O., Goldstein, J.S. Block, M.J., 1959, The motion of bubbles in a vertical temperature gradient, *Journal of Fluid Mechanics,* vol. 6, pp. 350.

[3] Trefethen, L., 1964, Surface Tension in Fluid Mechanics, *Educ. Serv. Inc. For Nat. Comm. of Fluid Mechanics Films.*

[4] McGrew, J.L., Bamford, F.L., Rehm, T.R., 1966, Marangoni flow: An additional mechanism in boiling heat transfer, *Science* 153, pp. 1106.

[5] Larkin, B.K., 1970, Thermocapillary flow around hemispherical bubble. *A.I.Ch.E. Journal* 16, pp. 101-107.

[6] Gaddis, E.S., 1972, The effect of liquid motion induced by phase change and thermocapillarity on the thermal equilibrium of a vapour bubble, *International Journal of Heat and Mass Transfer*, vol. 15, pp. 2241-2250.

[7] Kao, Y.S., Kenning, D.B.R., 1972, Thermocapillary flow near a hemispherical bubble on a heated wall, *Journal of Fluid Mechanics*, vol. 53, pp. 715-735.

[8] Sáiz Jabardo, J.M., Jones, B.G., 1981, A numerical investigation on thermocapillary flow around a hemispherical, non-condensable gas bubble, *20th National Heat Transfer Conference ASME/AIChE, Milwaukee, USA.*

[9] Straub, J., 1994, The role of surface tension for two phase heat and mass transfer in the absence of gravity, *Experimental Thermal and Fluid Science*, vol. 9, pp. 253-273.

[10] Straub, J., Betz. J., Marek, R., 1994, Enhancement of heat transfer by thermocapillary convection around bubbles: A numerical study, *Numerical Heat Transfer*, Part A, 25(5), pp. 501-518.

[11] Marek, R., Straub, J., 2001, The origin of thermocapillary convection in subcooled nucleate pool boiling, *International Journal of Heat and Mass Transfer*, vol. 44, pp. 619-632.

[12] Betz, J., Straub, J., 2001, Numerical and experimental study of the heat transfer and fluid flow by thermocapillary convection around gas bubbles, *Heat and Mass Transfer*, vol. 37, pp. 215-227.

[13] Arlabosse, P., 1997, Etude des transferts de chaleur et de masse par effect Marangoni: Application à la conpréhension des mécanismes de l'ebullition en apesanteur, *Ph. D. Thesis, University of Provence, Marseille, France.*

[14] Arlabosse, P., Lock, N., Medale, M., Jaeger, M., 1999, Numerical investigation of thermocapillary flow around a bubble, *Physics of Fluids*, vol. 11, pp. 18-29.

[15] Arlabosse, P., Tadrist, L., Tadrist, H., Pantaloni, J., 2000, Experimental analysis of the heat transfer induced by thermocapillary convection around a bubble, *Journal of Heat Transfer*, vol. 122, pp. 66-73.

[16] Peng, X.R., Huang, Y.J., Lee, D.J., 2001, Transport phenomenon of a vapour bubble attached to a downward surface, *International Journal of Thermal Sciences*, vol. 40, 9, pp. 797-803.

[17] Wang, H., Peng, X.F., Lin, W.K., Pan, C, Wang, B.X., 2004, Bubble-top jet flow on microwires, *International Journal of Heat and Mass Transfer,* vol. 47, 2891-2900.

[18] Wang, H. Peng, X.F. Christopher, D.M. Lin W.K., Pan, C., 2005, Investigation of bubble-top jet flow during subcooled boiling on wires, *International Journal of Heat and Fluid Flow*, vol. 26, pp. 485-494.

[19] Lu, J.F., Peng, X.F., 2007, Bubble jet flow formation during boiling of subcooled water on fine wires, *International Journal of Heat and Mass Transfer*, vol. 50, pp. 3966-3976.

[20] O`Shaughnessy, S.M., Robinson, A., 2008, Numerical investigation of bubble induced Marangoni convection: Some aspects of bubble geometry, *Microgravity Science and Technology*, vol. 20, pp. 319-325.

[21] Radulescu, C., Robinson, A., 2008, The influence of gravity and confinement on Marangoni flow and heat transfer around a bubble in a cavity: A numerical study, *Microgravity Science and Technology*, vol. 20, pp. 253-259.

[22] Lamas Galdo, M.I., Sáiz Jabardo, J.M., Arce Ceinos, A., Investigação numérica da termocapilaridade ao redor de uma bolha de gas não-condensável, *II Jornada Luso-Brasileira de Ensino e Tecnologia em Engenharia – JLBE 2009.*

[23] Lamas Galdo, M.I., Sáiz Jabardo, J.M., Arce Ceinos, A., Análisis numérico transitorio alrededor de una burbuja de gas no condensable, *VI Jornadas Nacionales de Ingeniería Termodinámica, JNIT 2009.*

[24] FLUENT 6.3 Documentation, 2006, FLUENT Inc.